Black hole-neutron star mergers for $10M_\odot$ black holes

Francois Foucart,[1,2] Matthew D. Duez,[3] Lawrence E. Kidder,[1] Mark A. Scheel,[4] Bela Szilagyi,[4] and Saul A. Teukolsky[1]

[1]*Center for Radiophysics and Space Research, Cornell University, Ithaca, New York, 14853, USA*
[2]*Canadian Institute for Theoretical Astrophysics, University of Toronto, Toronto, Ontario M5S 3H8, Canada*
[3]*Department of Physics & Astronomy, Washington State University, Pullman, Washington 99164, USA*
[4]*Theoretical Astrophysics 350-17, California Institute of Technology, Pasadena, California 91125, USA*

General relativistic simulations of black hole-neutron star mergers have currently been limited to low-mass black holes ($M_{\rm BH} \leq 7M_\odot$), even though population synthesis models indicate that a majority of mergers might involve more massive black holes ($M_{\rm BH} \geq 10M_\odot$). We present the first general relativistic simulations of black hole-neutron star mergers with $M_{\rm BH} \sim 10M_\odot$. For massive black holes, the tidal forces acting on the neutron star are usually too weak to disrupt the star before it reaches the innermost stable circular orbit of the black hole. Varying the spin of the black hole in the range $a_{\rm BH}/M_{\rm BH} = 0.5 - 0.9$, we find that mergers result in the disruption of the star and the formation of a massive accretion disk only for large spins $a_{\rm BH}/M_{\rm BH} \geq 0.7 - 0.9$. From these results, we obtain updated constraints on the ability of BHNS mergers to be the progenitors of short gamma-ray bursts as a function of the mass and spin of the black hole. We also discuss the dependence of the gravitational wave signal on the black hole parameters, and provide waveforms and spectra from simulations beginning $7 - 8$ orbits before merger.

I. INTRODUCTION

The study of black hole-neutron star (BHNS) mergers offers an opportunity to observe a general relativistic system in the strong field regime, in the presence of material at supernuclear density, magnetic fields, shocks, and intense neutrino radiation. As for other compact binaries, recent interest in black hole-neutron star systems is due in large part to their potential as sources of gravitational waves detectable by the next generation of ground-based detectors, Advanced LIGO [1] and VIRGO [2]. Indeed, whether for detection or parameter estimates, these detectors require theoretical templates in order to extract the gravitational wave signal from the detector noise. And in the orbits immediately preceding the merger, as during the merger itself, these binaries can only be properly modeled by numerical simulations in general relativity.

The emission of gravitational waves is not the only interesting feature of BHNS mergers, however. For compact binaries containing at least one neutron star the outcome of the merger is by itself an important question. The formation around the remnant black hole of a massive, thick, and hot accretion disk from the remains of a tidally disrupted neutron star offers ideal conditions to power short-hard gamma ray bursts (SGRB). This possibility, combined with the association of SGRBs with relatively old stellar populations, makes BHNS and NS-NS mergers some of the most likely progenitors of SGRBs (see e.g. [3] for a review).

Black hole-neutron star binaries have not yet been as widely studied as NS-NS or BH-BH systems. The first simulation of a BHNS merger in general relativity was done in 2006 by Shibata & Uryu [4]. Since then, various groups have studied the influence on the dynamics of the merger and the gravitational wave signal of the black hole spin [5–7], the mass ratio [5, 7, 8], the neutron star equation of state [7–10], the eccentricity of the orbit [11], and the presence of a magnetic field [12]. A review of those results can be found in [13]. These simulations indicate that mergers of low-eccentricity BHNS binaries show two potential qualitative behaviors. In the first, the neutron star is tidally disrupted before it reaches the innermost circular orbit (ISCO) of the black hole. Material from the star is then either quickly accreted onto the black hole, or ejected in a long tidal tail. As material in the tail falls back onto the black hole, it then forms an accretion disk. These disks are usually fairly thick, have temperatures of a few MeV, can contain a significant fraction of the initial mass of the star (a few tenths of a solar mass), and maintain a baryon-free region along the rotation axis of the black hole in which relativistic jets could be launched. They therefore offer promising conditions for the generation of SGRBs. The second scenario lets the star reach the ISCO before it overflows its Roche lobe. No tidal tail is formed, and the black hole and neutron star merge directly. Numerical simulations have confirmed that disk formation is favored by a high black hole spin (as the ISCO is closer to the black hole), a large neutron star (the star is more easily disrupted), and a small black hole mass (the size of the Roche lobe at the ISCO relative to the radius of the neutron star is smaller for lower mass black holes, thus making Roche-lobe overflow easier).

All existing simulations of BHNS mergers in general relativity have studied black holes of mass between 2 and 5 times the mass of the neutron star. For such configurations, disk formation is the most likely scenario. It can only be prevented for anti-aligned spins [5, 7], and compact stars or massive non-spinning black holes [5, 10]. However, the choice of such low mass ratios is not very well motivated. Population synthesis models tend in fact to favor distributions in which a large fraction of BHNS binaries have a more massive black hole ($M_{\rm BH} \geq 10M_\odot$), especially for binaries formed in low-metallicity environments [14, 15]. These predictions come with large uncertainties, but it still appears important to study the behavior of BHNS systems for higher mass black holes.

Simulations of binary systems with high mass ratios are typically more costly than their equal-mass counterparts. The reason is that before disruption the time step of the evolu-

tion is limited by the minimum spacing of the numerical grid (Courant-Friedrichs-Lewy condition), which scales as the size of the smaller object. High mass ratio simulations thus require significantly more time steps per orbit if we want to maintain the same accuracy. Mergers are also more difficult in this case: the rapid accretion of matter onto the black hole from a relatively small object can only be resolved if the numerical grid around the black hole has an accordingly small spacing, and a small time step is thus required as well. These increasing costs, plus the fact that lower mass ratios offer richer physical effects, have led to a focus on low black hole masses in general relativistic simulations of BHNS mergers up till now. High-mass ratio BHNS binaries have, however, been evolved using approximate treatments of gravity (e.g. in [16–19]). These simulations tend to indicate that high spins are required for disk formation to be possible. However, approximate simulations have been known to disagree with results in full general relativity in the past, especially on predictions regarding the mass of the accretion disk or the amount of unbound material ejected in the tidal tail.

In this paper, we focus on the features of BHNS mergers for black holes of mass $7 - 10 M_\odot$. In Section II, we review our numerical code and the specific challenges related to the evolution of high mass ratio systems, and describe recent improvements to our code. We also present updated diagnostics regarding the accuracy of our gravitational wave-forms, and the influence of gauge choices on our results. Section III describes the initial conditions for our simulations, while Section IV presents our numerical results. In particular, we show that for massive black holes ($M_{BH} \geq 10 M_\odot$), disks cannot be formed unless the spin of the black hole is high ($a_{BH}/M_{BH} \geq 0.7$). We also discuss the imprint of the binary parameters on the gravitational wave signal. Finally, Section V focuses on consequences for the observation of SGRBs.

II. METHODS AND DIAGNOSTICS

The black hole-neutron star binaries presented in this paper are evolved using the numerical code developed by the SpEC collaboration [20]. The coupled system formed by Einstein's equations and the general relativistic hydrodynamics equations is solved using the two-grid method described in Duez et al. [21], with the improvements discussed in Foucart et al. [6]. We refer the reader to [21] for a detailed description of the numerical methods used in SpEC, and only discuss here some recent modifications improving the general performance of the code, and facilitating the merger of high mass ratio BHNS binaries.

In the two-grid method, Einstein's equations are solved within the generalized harmonic formalism [22] using pseudospectral methods, while the fluid equations are evolved on a separate finite difference grid. This allows us to take advantage of the efficiency of pseudospectral methods for the evolution of Einstein's equations in regions in which the solution is smooth (i.e., away from the neutron star), while limiting the extent of the finite difference grid to regions in which matter

is present. The price to pay is that, as the two sets of equations are coupled, source terms have to be interpolated between the two grids at each time step.

The relativistic hydrodynamics equations are solved in conservative form: the evolved conservative variables $\boldsymbol{U}$ satisfy equations of the form

$$\partial_t \boldsymbol{U} + \nabla \cdot \boldsymbol{F}(\boldsymbol{U}) = \boldsymbol{S}(\boldsymbol{U}), \tag{1}$$

where the fluxes $\boldsymbol{F}$ and source terms $\boldsymbol{S}$ are functions of the variables $\boldsymbol{U}$ but not of their derivatives. A conservative shock-capturing scheme is characterized by a reconstruction method, whereby fluid quantities on either side of cell faces are constructed, and a Riemann solver that supplies the resulting fluxes across each cell face. For these simulations, we use 5th-order WENO reconstruction [23, 24] with the smoothness indicator proposed by Borges et al [25] and HLLE fluxes [26].

Since the publication of Foucart et al. [6], other modifications of the SpEC code have significantly improved the efficiency of our simulations. In the following sections, we discuss the most important of these recent changes.

A. Adaptive time stepper

In previously published simulations, black hole-neutron star binaries were evolved using a fixed time step $\Delta t = C \Delta x_{min}$, where Δx_{min} is the smallest grid spacing and C some constant chosen so that the evolution satisfies the Courant-Friedrichs-Lewy (CFL) stability condition at all times. As the truncation error in these simulations is usually dominated by the effects of the spatial discretization, this is sufficient for the effects of the discretization in time to be negligible. However, the resulting time step can be significantly smaller than necessary for a large fraction of the evolution. Indeed, the maximum value of C that gives stable evolutions can change over time[1] and is a priori unknown for the evolution of Einstein's equations on a pseudospectral grid. Additionally, the only way to confirm that the error in a given simulation is indeed dominated by spatial truncation error is to rerun it with a different choice for C. Using an adaptive time stepper, we instead choose at any time the largest time step for which the time stepping error is smaller than some tolerance. If the CFL instability begins to grow, this shows up as an increasing time stepping error and the time stepper automatically reduces the time step. In practice, time step control is done by evaluating the time stepping error through comparisons of the result of the time evolution with what would be obtained if a lower order scheme were used. We evolve using the 3rd-order Runge-Kutta algorithm, and compare with the results of a second-order method. The time step h_{n+1} is then determined using a proportional-integral (PI) stepsize control [27–30]:

$$h_{n+1} = S h_n \epsilon_n^{-\alpha} \epsilon_{n-1}^\beta \tag{2}$$

---

[1] The variation in time of the CFL stability condition occurs mainly because the pseudospectral grid follows the evolution of the binary and, in particular, contracts as the binary spirals in.

where ϵ_n is the error measured at time step n, $S = 0.9$ is a safety factor, $\beta \approx 0.13$ and $\alpha \approx 0.23$.

For the evolution of a BHNS binary over $7 - 8$ orbits, choosing the optimal Δt at all times can reduce the simulation time by a factor of $\sim 1.5 - 2$. Additionally, as the minimum value of C giving stable evolutions is unknown, our choice when using fixed time steps was usually overly cautious. The actual gain in the time required to evolve BHNS systems with SpEC at a given resolution is thus closer to a factor of $2 - 3$.

B. Control system

The evolution of a black hole on a pseudospectral grid requires the excision of the region surrounding the singularity. As a consequence, the numerical domain has an inner boundary $\mathcal{S}_{\rm in}$, typically a sphere in the coordinates of the numerical grid. If any information can enter the domain through $\mathcal{S}_{\rm in}$, an unknown boundary condition has to be imposed there. Inside the apparent horizon of the black hole, this can however be avoided for 'good' choices of $\mathcal{S}_{\rm in}$. More specifically, we compute the local characteristic speeds of the generalized harmonic equations (which are hyperbolic), and require that on $\mathcal{S}_{\rm in}$ all characteristic speeds point out of the numerical grid. We also require that $\mathcal{S}_{\rm in}$ remain inside the apparent horizon of the black hole. In practice, this can be difficult when the black hole is rapidly evolving through tidal distortion or matter accretion. During merger, we try to keep the apparent horizon nearly spherical in the coordinates of the numerical grid, and slightly outside $\mathcal{S}_{\rm in}$, through the use of a coordinate map between the grid coordinates and the inertial frame:

$$\tilde{r} = r(1 + \sum_{lm} Y_{lm}(\theta, \phi)c_{lm}), \tag{3}$$

where $\tilde{r}$ is the distance from the black hole center in the inertial frame, r the same distance in the grid coordinates, (θ, ϕ) the usual angles in spherical coordinates (in both frames), and c_{lm} arbitrary coefficients used to control the location of $\mathcal{S}_{\rm in}$ in the grid frame. The quantity c_{00} thus controls the size of $\mathcal{S}_{\rm in}$, while the other coefficients control its shape. In previous simulations, the control system attempted to choose the c_{lm} so that the apparent horizon remained a sphere of fixed radius in the grid frame. This proved inadequate for high mass ratio simulations: there is a priori no way to know at what distance the apparent horizon should be kept from $\mathcal{S}_{\rm in}$, and making the wrong choice can easily lead to characteristic speeds entering the domain on $\mathcal{S}_{\rm in}$. Instead, we now choose c_{00} by using the characteristic speeds themselves as input for the control system. Indeed, $\partial_t c_{00}$ affects the velocity of the surface $\mathcal{S}_{\rm in}$ in inertial coordinates, and can thus be used to increase or decrease the characteristic speeds at will. The other coefficients are still chosen so that the apparent horizon remains spherical.

As the time scale over which $\mathcal{S}_{\rm in}$ needs to change varies by orders of magnitude between the early orbits and the merger, the control system used to fix the c_{lm} has also been modified in order to choose adaptively the time scale over which it attempts to damp any deviation of the motion of $\mathcal{S}_{\rm in}$ from its desired behavior.

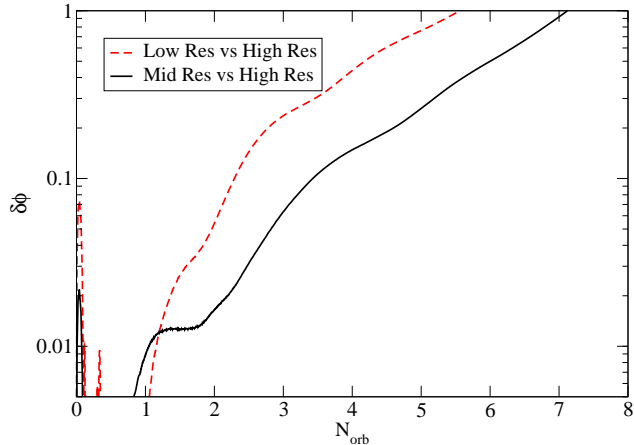### C. Adaptive Mesh Refinement on the spectral grid

Another complication arising for high mass ratio mergers is the rapid motion of the high-density neutron star core across the numerical grid as it falls into the black hole. This high-density material generates large source terms in Einstein's equations, which vary quickly and can have very steep gradients. Maintaining a grid resolution high enough to resolve these features in all parts of the numerical domain where they might occur, and during the entire simulation, is far too costly to be realistic. In practice, we need to adapt the numerical domain at regular time intervals in order to increase resolution in regions where the neutron star core is located. This was already done on the finite difference grid, by limiting the grid to regions in which matter is present [6]. The possibility of modifying the pseudospectral grid during a simulation, on the other hand, is a new feature of our code which was initially developed to improve the accuracy of black hole binary mergers. The choice of how to modify the resolution in any given subdomain of the numerical grid relies on estimates of the truncation error based on the fall-off rate of the coefficients of the spectral expansion. For a smooth solution, these coefficients should fall off exponentially. In BHNS simulations, the solution is not smooth, but the metric quantities are still continuous, and their spectral expansion converges as a power law. The determination of the required resolution is less reliable than in vacuum—and better methods to control that choice should be found if we want to take full advantage of the method—but in its current form this spectral adaptive mesh refinement (AMR) technique has already allowed us to evolve configurations that were otherwise too costly to simulate accurately. In this paper, spectral AMR is used for the merger of case Q7S5, the only configuration in which the neutron star merges without any significant tidal disruption.

D. Gravitational Wave Accuracy

Gravitational wave templates for ground based detectors such as Advanced LIGO require accurate waveforms. Even the longest and most accurate simulations of binary black holes combined with Post-Newtonian results to generate hybrid waveforms might currently be insufficient for precise parameter estimates (i.e., the accuracy of the parameters might be limited by the quality of the templates instead of the noise in the LIGO data) [31, 32]. Templates could well require a phase accuracy in the numerical waveform of $0.1 \, \rm rad$ over significantly more than the 30 cycles of the longest available numerical waveform [32]. Accuracy requirements are lower for detection purposes, and some parameters could be usefully constrained with waveforms at the current level of accuracy (e.g., the neutron star radius from NS-NS mergers [33]). But it is clear that template accuracy is a significant concern for gravitational wave astronomy.

Binary neutron stars and BHNS binaries are particularly challenging, as the need to evolve the neutron star fluid adds new sources of errors to the simulations. In previous papers [6, 9], we evolved the system for only $2 - 3$ orbits before

FIG. 1: Phase error $\delta\phi$ for the (2,2) mode of the gravitational wave signal as a function of the number of orbits, for simulation Q7S7. The wave is extracted at finite radius $R = 100M_{\text{total}}$, and we do not attempt to shift it in phase or time.

FIG. 2: (2,2) mode of the strain h for simulation Q7S7 at our two highest resolutions, extracted at finite radius $R = 100M_{\text{total}}$. We shift the signal in time and phase so that the phase at the peak of the signal is $\phi = 0$, and the time $t = 0$.

merger, and the phase error in the gravitational wave signal was of the order of a few tenths of a radian even before merger. The simulations presented here are significantly longer ($7-8$ orbits), and more accurate (the 'low' resolution used here is roughly equivalent to our standard resolution in [6]). We thus need to reassess the accuracy of our waveforms.

The error in the gravitational wave signal is evaluated using the Q7S7 simulation ($q = 7$, $a_{\text{BH}}/M_{\text{BH}} = 0.7$), which we run at 3 different resolutions. The gravitational wave signal is extracted at finite radius $R = 100M_{\text{tot}}$, where $M_{\text{tot}} = M_{\text{BH}} + M_{\text{NS}}$. We directly compute the strain h expended in spherical harmonics ($h = \sum_{lm} h_{lm} Y_{lm}$), using the Regge-Wheeler-Zerilli method [34–37]. In Fig. 1, we show the raw phase difference between our high resolution simulation and the lower resolution simulations for the dominant h_{22} mode. The phase is directly extracted from the real and imaginary parts of h_{22}, without any time or phase shift. The phase error in the low resolution case reaches $0.2\,\text{rad}$ after only 2.5 orbits, as expected from the fact that it is equivalent to the resolution used in [6]. At higher resolution, however, the same phase difference is only reached after approximately 4.5 orbits, and the overall accuracy is significantly better up to merger even though by then the phase shift is of the order of a radian.

Such errors are typical of current general relativistic simulations. We can, for example, compare our results with those of the most recent BHNS mergers of Kyutoku et al. [7]. There, the error in the waveform is measured after applying a shift in time and phase. This is justified from an observational point of view by the fact that a detector would not be sensitive to such shifts, even though it might also give an optimistic view of the uncertainties at the time of merger. Fig. 2 shows the wave from the two highest resolution of simulation Q7S7, but shifted so that the time at which the signal peaks is $t = 0$ and the phase at that time is $\phi = 0$. The errors appear comparable to Fig.25 of [7], and significantly smaller than the differences due to changes in the parameters of the binary, discussed in Sec. IV B.
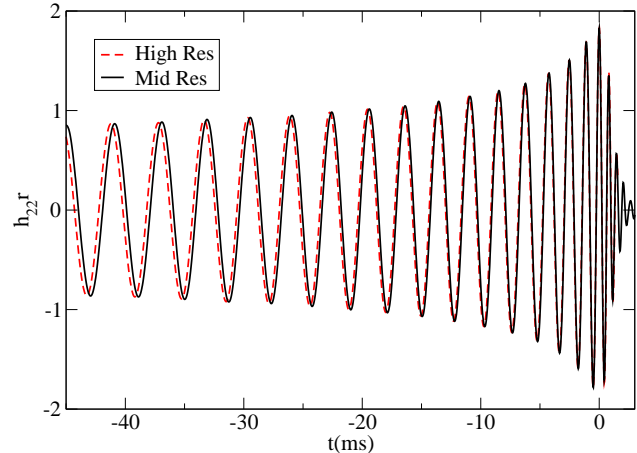
E. Gauge dependence

In the generalized harmonic formulation, the gauge is specified through a choice of the variable $H_a = g_{ab}\nabla_c\nabla^c x^b$. For most runs reported here, we evolve this function as in our previous work [6]. During the inspiral, we fix H_a in the comoving frame at its initial value. During the merger, we continue to fix H_a near the black hole; away from the hole, we damp it to zero. Because this gauge is presumably not optimal for the merger evolution near the black hole, significant grid stretching is expected and found during this part of the evolution. To test whether the gauge behavior significantly affects the accuracy of the simulations, we reran the merger phase of the Q5S5 runs using the damped-wave gauge introduced by Szilágyi, Lindblom, and Scheel [38]. The resulting metric evolution is, of course, different (and noticeably more moderate), but the gravitational wave signal should be the same. To within numerical errors, this is indeed what we find. Also, the difference in waveform between resolutions is comparable for each gauge, indicating that grid distortion is not the major source of waveform error.

III. INITIAL CONFIGURATIONS

We generate initial data for our simulations with the elliptic solver SPELLS [39]. To obtain realistic initial configurations for the evolution of black hole-neutron star binaries, we have to satisfy the constraints in Einstein's equations, as well as choose a realistic initial state for the fluid forming the neutron star. For the fluid we require hydrostatic equilibrium as well as an irrotational velocity profile. The procedure for solving for these conditions and obtaining compact objects with the desired masses, spins and orbital parameters is detailed in Foucart et al. [40]. The constraint equations are solved in the extended conformal thin sandwich formalism [41, 42]. In that

formalism, the metric is decomposed as

$$ds^2 = g_{\mu\nu}dx^\mu dx^\nu = -\alpha^2 dt^2 + \phi^4\tilde{\gamma}_{ij}(\beta^i dt + dx^i)(\beta^j dt + dx^j) \tag{4}$$

where α is the lapse function, β^i the shift vector, $\tilde{\gamma}_{ij}$ the conformal 3-metric and ϕ the conformal factor. The constraints can then be expressed as elliptic equations for $(\alpha\phi, \beta^i, \phi)$. The choice of the conformal metric, the trace of the extrinsic curvature $K_{\mu\nu} = -\frac{1}{2}\mathcal{L}g_{\mu\nu}$, and their time derivatives is then arbitrary. Together with the boundary conditions and the stress-energy tensor, these arbitrary choices will determine the characteristics of the spacetime under consideration. A standard choice in the literature is $\tilde{g}_{ij} = \delta_{ij}$, $K = 0$. However, for high black hole spins this leads to configurations far from equilibrium, and potentially large modifications of the black hole spin and mass at the beginning of the simulation. We prefer to choose the free data (g_{ij}, K) according to the prescription of Lovelace et al. [43]: close to the horizon of the BH, the metric matches the Kerr-Schild solution. (For the adaptation of that method to BHNS systems, see [40].)

In this paper, we are interested in the behavior of BHNS binaries for high mass ratio $q = M_{BH}/M_{NS} = 7$. We consider 4 different configurations, summarized in Table I. The first is at a slightly lower mass ratio $q = 5$, a range of masses already explored by Etienne et al. [5], Kyutoku et al. [7] and Chawla et al. [12]. The spin of the black hole is $a_{BH}/M_{BH} = 0.5$, aligned with the orbital angular momentum of the binary. The other three simulations use $q = 7$. We show in Sec. IV A that these cases span the range of BH spins over which the qualitative features of the merger vary: $a_{BH}/M_{BH} = 0.5, 0.7, 0.9$. All configurations are started approximately 8 orbits before disruption, and have low eccentricity $e \leq 0.005$ (obtained using the iterative method developed by Pfeiffer et al. [44]). For the equation of state of nuclear matter, we choose a polytrope: the pressure P and internal energy ϵ are expressed as functions of the baryon density ρ_0 and temperature T:

$$P = \kappa\rho_0^\Gamma + \rho_0 T \tag{5}$$
$$\epsilon = \frac{P}{\rho_0(\Gamma - 1)}, \tag{6}$$

with $\Gamma = 2$ and κ chosen so that the compaction of the star is $C = M/R = 0.144$. This corresponds to a stellar radius $R \sim 14.4\,\mathrm{km}$ for a $1.4M_\odot$ neutron star. Recent predictions regarding the radius of neutron stars indicate that this is probably close to an upper bound on the radius of real stars (see, e.g., [45]).

We use three different resolutions: 80^3, 100^3 and 120^3 points on the finite difference grid (which only covers the neutron star), and 56.9^3, 64.5^3 and 72.0^3 points on the pseudospectral grid. At the highest resolution on a moderate size cluster, 8 orbits require approximately $40,000$ CPU-hrs (about a month on 48 processors). During mergers, the resolution of both the finite difference and pseudospectral grids is higher, and depends on the configuration studied.

TABLE I: Initial configurations studied. a_{BH}/M_{BH} is the dimensionless BH spin, $M_{BH,NS}$ the ADM masses of equivalent isolated BH and NS, R_{NS} the radius of the star, Ω_{rot}^0 the initial angular frequency of the orbit, M_{tot} the ADM mass of the system at infinite separation, and e the initial eccentricity. The number of orbits N_{orbits} is measured at the point at which 10% of the mass has been accreted by the black hole.

| Name	$\frac{M_{BH}}{M_{NS}}$	$\frac{a_{BH}}{M_{BH}}$	$C = \frac{M_{NS}}{R_{NS}}$	$\Omega_{rot}^0 M_{tot}$	N_{orbits}	e
Q7S5	7	0.5	0.144	3.84e-2	7.7	0.001
Q7S7	7	0.7	0.144	4.14e-2	8.3	0.004
Q7S9	7	0.9	0.144	4.47e-2	8.8	0.005
Q5S5	5	0.5	0.144	3.55e-2	7.2	0.003

IV. RESULTS

A. Mergers

Most existing simulations of BHNS mergers with lower mass black holes ($M_{BH} \sim 3 - 7M_\odot$) show very similar qualitative behavior. As the neutron star gets close to the black hole, tidal forces cause the star to overflow its Roche lobe. Most of the matter is either rapidly accreted onto the black hole, or ejected into an extended tidal tail. Material in the tidal tail then rapidly forms a thick and hot accretion disk around the black hole ($T \sim 1 - 5\,\mathrm{MeV}$). To obtain different behaviors, one must consider either highly eccentric orbits [11]—in which case partial disruption of the neutron star is possible—or anti-aligned black hole spins [5], where it becomes possible to directly accrete the entire neutron star since it reaches the innermost stable circular orbit before overflowing its Roche lobe. Negligible disk masses are also observed for nonspinning black holes and fairly compact stars at the high end of the range of studied BH mass ($q = 4 - 5$) [5, 7].

The situation changes significantly when considering more massive black holes, $q \sim 7$. For such binaries, the standard behavior appears to be the direct merger of the two compact objects, without significant tidal disruption of the stars. The simulations presented in this paper use neutron stars with radii on the high end of the theoretically acceptable values. This is known to favor tidal disruption [7–9], as material on the surface is less tightly bound to the neutron star. Even so, in our lower spin simulation ($q = 7$, $a_{BH}/M_{BH} = 0.5$), 99% of the material falls into the black hole in less than $2\,\mathrm{ms}$. Snapshots of the matter configuration for that simulation are given in Fig. 3. Once accretion begins, most of the neutron star material remains within a coordinate distance of less than about $40\,\mathrm{km}$ from the center of the black hole, and only a negligible amount of matter forms a tidal tail (approximately 0.5% of the NS mass). As spin misalignment, a lower spin and a more compact neutron star all work against tidal disruption, this gives us a strict lower bound on the black hole spin required to disrupt the star for black holes with mass $M_{BH} \geq 7M_{NS}$.

When the spin of the black hole is increased to $a_{BH}/M_{BH} = 0.7$, the disruption of the neutron star becomes clearly visible (Fig. 4, left). A long tidal tail extending more than $100\,\mathrm{km}$ away from the black hole and containing about 8% of the initial mass of the star is created from the ejected

FIG. 3: Matter distribution for simulation Q7S5. *Left:* Most of the neutron star material plunges directly into the black hole at the time of merger. Density contours: $\rho_0 = (10^{14}, 10^{13}, 10^{12}, 10^{11}, 10^{10}) \, \text{g/cm}^3$. *Right:* 1ms later, only 2% of the neutron star material remains outside the black hole, and most of it will rapidly accrete onto the hole. Density contours: $\rho_0 = (10^{12}, 10^{11}, 10^{10}) \, \text{g/cm}^3$.
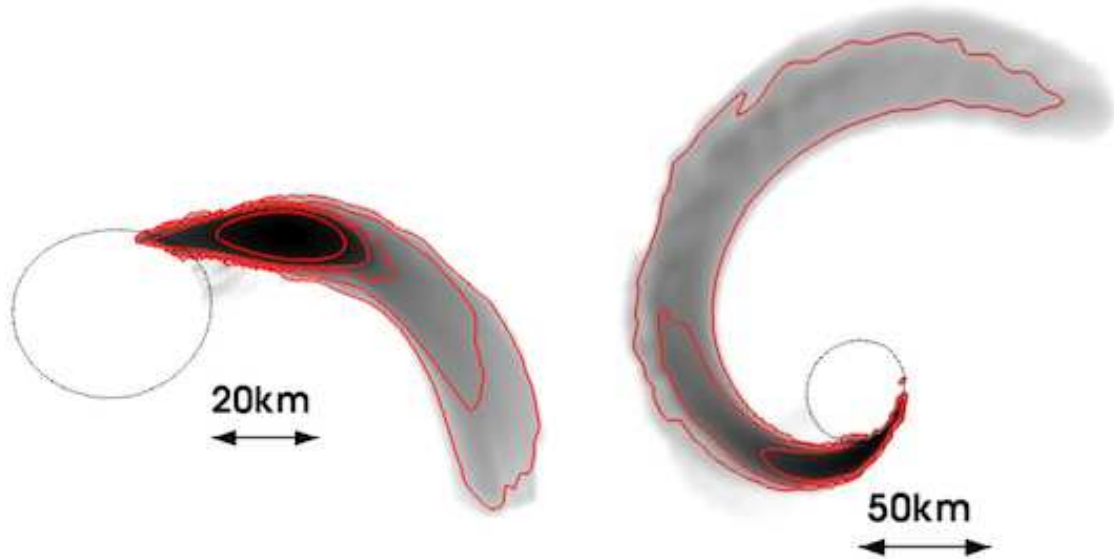
material. About $5 \, \text{ms}$ after disruption, a proto-accretion disk forms (Fig. 4, center). However, the disk contains only a fairly small portion of the ejected material, and is still thinner ($H/R \sim 0.1$, where H is the half-thickness of the disk) and colder ($T < 1 \, \text{MeV}$) than what is usually observed in mergers with less massive black holes.

Rapid accretion from the tidal tail prevents the disk from reaching an equilibrium profile for about $20 \, \text{ms}$. By that point, only 2.5% of the baryonic mass remains outside the black hole (Fig. 4, right). As the radius of the disk is about $100 \, \text{km}$, its density is much lower than in the case of higher black hole spins (see below) or lower black hole masses: the maximum density is only about $2 \times 10^{10} \, \text{g/cm}^3$. The thickness ($H/R \sim 0.3$) and temperature ($T \sim 2 \, \text{MeV}$) of the disk are closer to the equilibrium values found for $q = 3$ [6], but this still appears to be a less desirable configuration for the potential generation of a short gamma-ray burst.

This is no longer the case for the high spin configuration, $a_{\text{BH}}/M_{\text{BH}} = 0.9$. The disruption (Fig. 5, left) is very similar to the previous case, with a long tidal tail forming from the tidally disrupted star. However, now the disk can form much closer to the black hole because the innermost circular orbit is at a smaller radius. Also, the higher rotation speed of the hole prevents rapid accretion of high angular momentum material. Thus the amount of nuclear matter remaining outside of the black hole is now much larger: about 30% of the neutron star mass. Within approximately $5 \, \text{ms}$ of disruption, a large fraction of that material (about half) forms an accretion disk (Fig. 5, center) with stable density and angular momentum profiles.

The evolution of the resulting accretion disk is then similar to what is expected for lower mass black holes. The disk expands slightly, and heats up to $T \sim 5 - 6 \, \text{MeV}$, but does

TABLE II: Parameters of the final configuration. M_{disk} is defined as the mass available outside the black hole $5 \, \text{ms}$ after disruption. $a_{\text{BH}}/M_{\text{BH}}$ is the final dimensionless spin of the black hole. ρ_0^{max} is the maximum baryon density once the disk settles to an equilibrium configuration $20 \, \text{ms}$ after disruption. T is the average temperature and H is the semi-thickness of the disk at that time.

Name	$\frac{M_{\text{disk}}}{M_{\text{NS}}^0}$	$\frac{a_{\text{BH}}}{M_{\text{BH}}}$	$\rho_0^{\text{max}}(\frac{\text{g}}{\text{cm}^3})$	$T(\text{MeV})$	$\frac{H}{r}$	$v_{\text{k}}(\frac{\text{km}}{\text{s}})$
Q7S5	≤ 0.004	0.67		Not Applicable		86
Q7S7	0.06	0.80	2×10^{10}	2	0.3	63
Q7S9	0.28	0.92	3×10^{11}	6	0.3	39
Q5S5	0.06	0.71	8×10^{11}	2	0.3	106

not evolve much otherwise. The disk is thick ($H/R \sim 0.3$), and an order of magnitude denser than for $a_{\text{BH}}/M_{\text{BH}} = 0.7$. From the accretion rate at the end of the simulation, we deduce an expected lifetime of about $75 \, \text{ms}$, although this value would certainly be modified by the inclusion of magnetic effects. Another important feature of this high-spin case is that a few percent of the total mass appears to be either unbound or on orbits such that it will not interact with the accretion disk within its expected lifetime. As the outermost part of the tidal tail is poorly resolved in our simulations (the grid points are focused in the region close to the black hole where the accretion disk forms), predictions about the future of material ejected far away from the black hole are not very reliable. The mere presence of such material, however, indicates that massive ejecta might occur in BHNS mergers if the mass and spin of the black holes are high. By contrast, in previous simulations for lower BH masses or spins, all of the material in the tidal tail appeared unequivocally bound to the black hole.

The large differences in the amount of matter available outside the black hole as we modify the black hole spin

FIG. 4: Matter distribution for simulation Q7S7. *Left:* Disruption of the neutron star. Material that is not immediately accreted onto the black hole (about 8% of the NS mass) forms a thin tidal tail. Density contours: $\rho_0 = (10^{14}, 10^{13}, 10^{12}, 10^{11}, 10^{10})\,\mathrm{g/cm^3}$. *Center:* Disk formation, about 8ms later. A low density accretion disk begins to form about 50 km away from the black hole, but rapid mass accretion from the tidal tail causes the disk profile to vary significantly over time. The maximum density is $3 \times 10^{11}\,\mathrm{g/cm^3}$. Density contours: $\rho_0 = (10^{11}, 10^{10})\,\mathrm{g/cm^3}$. *Right:* About 20ms after disruption, a stable accretion disk has formed with low maximum density $\rho_{\max} \sim 2 \times 10^{10}\,\mathrm{g/cm^3}$. About 2.5% of the initial mass of the neutron star remains in the disk at that time, but accretion onto the black hole would destroy the disk within approximately 20 ms. Density contour: $\rho_0 = 10^9\,\mathrm{g/cm^3}$.
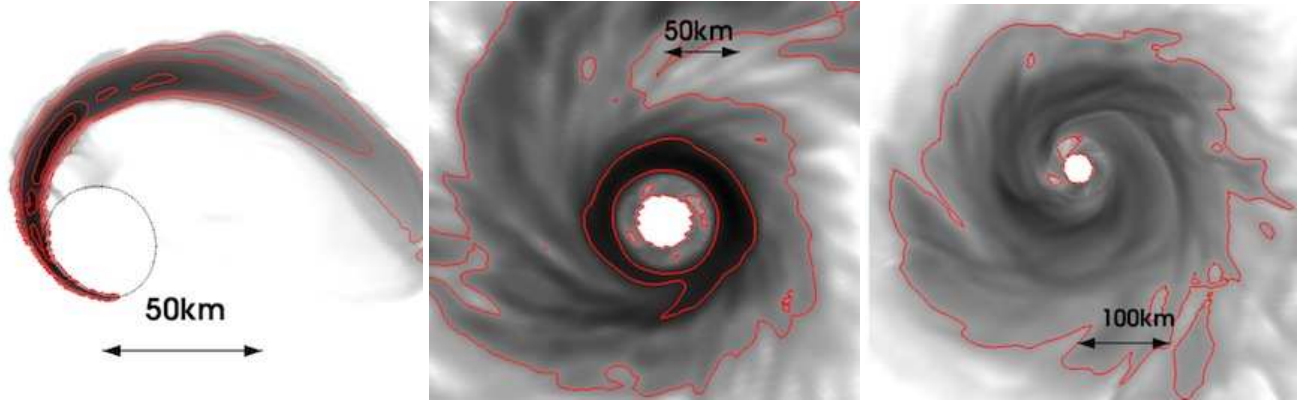
FIG. 5: Matter distribution for simulation Q7S9. *Left*: Disruption of the neutron star, very similar to the Q7S7 case (Fig. 4), but with more material ejected into the tidal tail. Density contours: $\rho_0 = (10^{14}, 10^{13}, 10^{12}, 10^{11}, 10^{10})\,\mathrm{g/cm^3}$. *Center:* Disk formation 6.5ms later. More than 25% of the fluid material remains outside the black hole. A massive accretion disk rapidly forms, containing more than 10% of the matter. Density contours: $\rho_0 = (10^{12}, 10^{11}, 10^{10})\,\mathrm{g/cm^3}$. *Right:* 20ms after disruption, a massive disk remains. It is 10 times denser than in the lower spin case, and has been in a nearly stable configuration for more than 10 ms. Density contours: $\rho_0 = (10^{11}, 10^{10})\,\mathrm{g/cm^3}$.
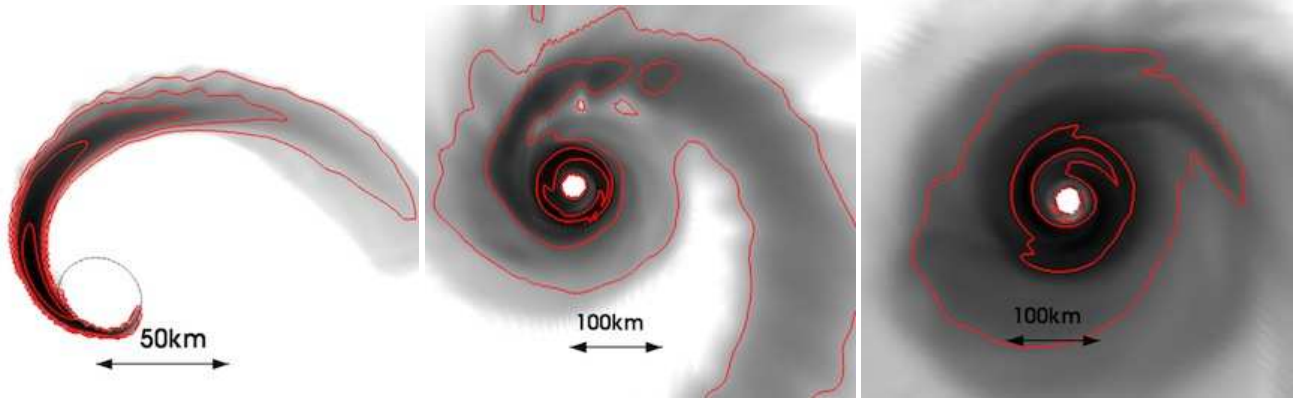

can be seen in Fig. 6. The figure shows the difference between a merger without disruption (Q7S5), with disruption followed by the slow formation of a low density, short-lived disk (Q7S7), and with disruption followed by the formation of a heavy, mostly stable accretion disk (Q7S9). For $M_{\mathrm{BH}}/M_{\mathrm{NS}} = 7$, we should thus expect strong qualitative differences in the behavior of BHNS mergers as we vary binary parameters such as the black hole spin or the NS equation of state, with a significant fraction of the parameter space now leading to direct merger of the binary without the formation of an accretion disk. From Fig. 6, we can also easily evaluate the influence of the black hole mass. The lower mass ratio simulation ($q = 5$), which has a black hole spin $a_{\mathrm{BH}}/M_{\mathrm{BH}} = 0.5$, behaves approximately as the $q = 7$, $a_{\mathrm{BH}}/M_{\mathrm{BH}} = 0.7$ case,

although the radius of the accretion disk around the less massive black hole is naturally smaller, and the maximum baryon density much higher. In Section V, we discuss in more detail how the qualitative behavior of BHNS mergers is affected by both the mass and spin of the black hole, and how this relates to their ability to power short gamma-ray bursts.

The results of the mergers are summarized in Table II. In addition to the disk mass and properties discussed above, Table II lists the final spin of the BH and the velocity kick imparted to the hole. As expected, the relative increase in the final black hole spin decreases as the initial spin of the black hole increases. Starting from a spin $a_{\mathrm{BH}}/M_{\mathrm{BH}} = 0.5$ leads to a final BH spin of 0.67, while an original spin of 0.9 only rises to 0.92 after merger. For low spins, the velocity kicks

FIG. 6: Baryon mass available outside the black hole as a function of time. The mass is normalized by the initial mass of the neutron star.
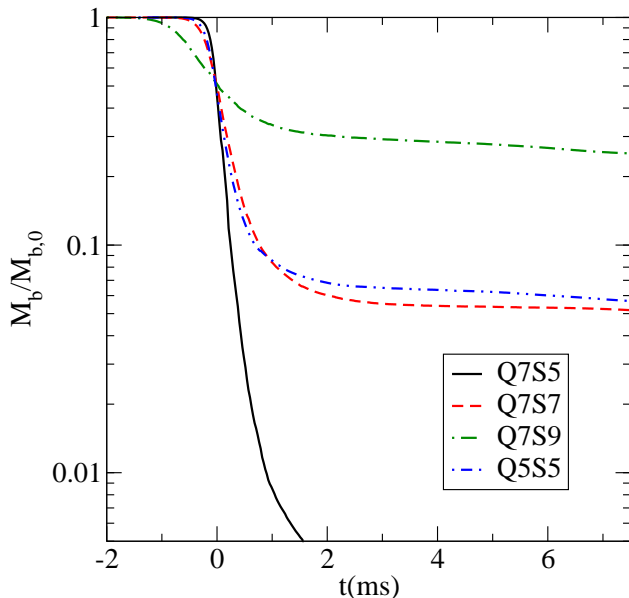
are close to binary black hole predictions [46, 47], but as we go to higher spins, the magnitude of the kick decreases. This could be expected, as most of the contribution to the kick in binary black hole mergers comes from the momentum radiated as gravitational waves just before merger, exactly the part of the signal that is not emitted by BHNS systems when the star is tidally disrupted before reaching the ISCO. The same effect was observed by Kyutoku et al. [7] at lower mass ratios.

B. Gravitational wave signal

The gravitational wave signal emitted as two compact objects spiral in and merge contains information on the orbital parameters of the binary, the masses and spins of the compact objects, and, in the presence of a neutron star, on the equation of state of matter above nuclear density. In BHNS binaries, as in BH-BH systems, these parameters leave a mark on the waveform as the binary spirals in. But on top of the information from the orbital evolution of the binary, BHNS systems also show strong variations in the qualitative features of the gravitational wave signal at the time of merger. This is visible on Fig. 7, which shows the gravitational strain measured for various binaries with $q = 7$ but different spins, and Fig. 8, which shows the same signals in the frequency domain. The low spin simulation Q7S5 has a spectrum qualitatively similar to that of a BH-BH binary : the power slowly decreases with increasing frequency as the binary spirals in, then peaks at the time of merger ($\sim 1\,\mathrm{kHz}$), and finally falls off exponentially as the remnant black hole rings down. At higher spins ($a_{\mathrm{BH}}/M_{\mathrm{BH}} \geq 0.7$), the neutron star disrupts and we no longer observe a peak in the gravitational wave spectrum. The high-frequency signal now depends on the details of the tidal disruption of the star. Lower spins lead to less disruption, with

FIG. 7: Gravitational wave signal for a mass ratio $q = 7$, when varying the black hole spin between $a_{\mathrm{BH}}/M_{\mathrm{BH}} = 0.5 - 0.9$. The time and phase of the waveforms are matched at the peak of the signal.
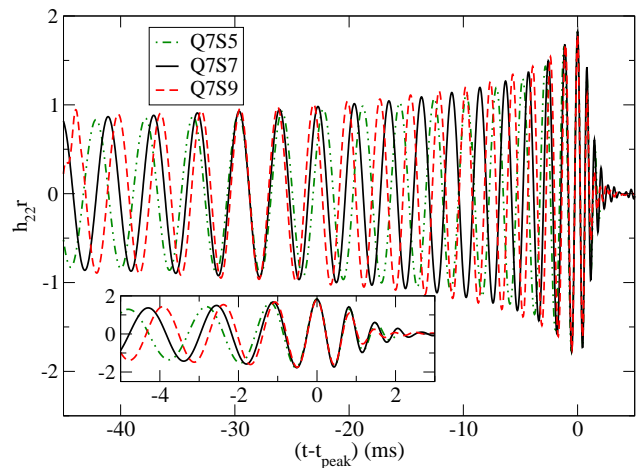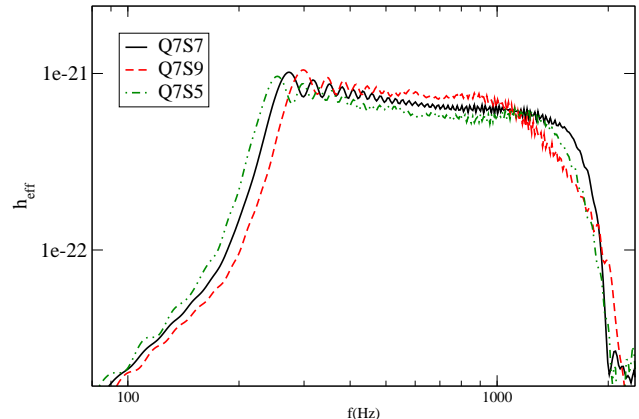

FIG. 8: Power spectrum of the gravitational wave signal for a mass ratio $q = 7$, while varying the black hole spin between $a_{\mathrm{BH}}/M_{\mathrm{BH}} = 0.5 - 0.9$. The cutoff at low frequency is only an effect of the finite length of the evolution. h_{eff} is the effective amplitude of the gravitational wave signal, as defined in Eq. (41) of [8].

most of the mass still falling rapidly into the black hole, while higher spins lead to more significant disruption, and a more homogeneous spread of the neutron star material around the black hole. Accordingly, high spin spectra are cut off at lower frequency, but fall off more smoothly. Similar qualitative differences are found by Kyutoku et al. [7] and Etienne et al. [5]. In fact, Fig. 8 is strikingly similar to Fig. 18 of [7], which shows the spectra of the gravitational wave signal for BHNS binaries with $q = 3$ and spins $a_{\mathrm{BH}}/M_{\mathrm{BH}} = -0.5, 0, 0.5$. Observationally, the effects of tidal disruption on the waveform are slightly easier to measure in the case of a high mass ratio, as the merger occurs at frequencies about a factor of 2 smaller than for $q = 3$ ($f \sim 1 - 1.5\,\mathrm{kHz}$), but this still remains a challenging frequency range for Advanced LIGO.

Figs. 9 and 10 show the gravitational wave signal of the two $a_{\mathrm{BH}}/M_{\mathrm{BH}} = 0.5$ simulations in the time and frequency domains. As expected from the above discussion, the lower mass

FIG. 9: Gravitational wave signal for the low spin simulations ($a_{BH}/M_{BH} = 0.5$) for mass ratios $q = (5, 7)$. The time and phase of the waveforms are matched at the peak of the signal.
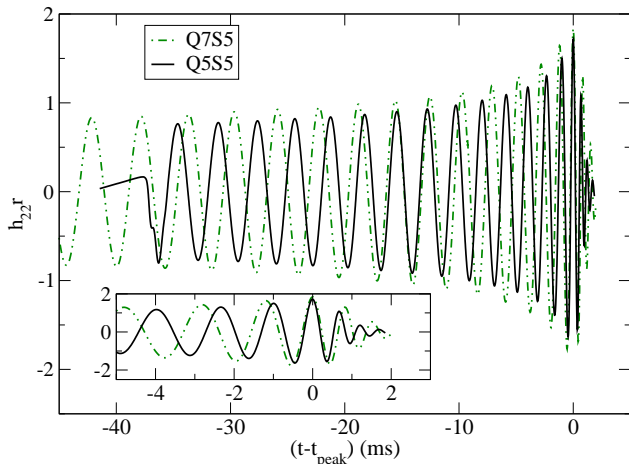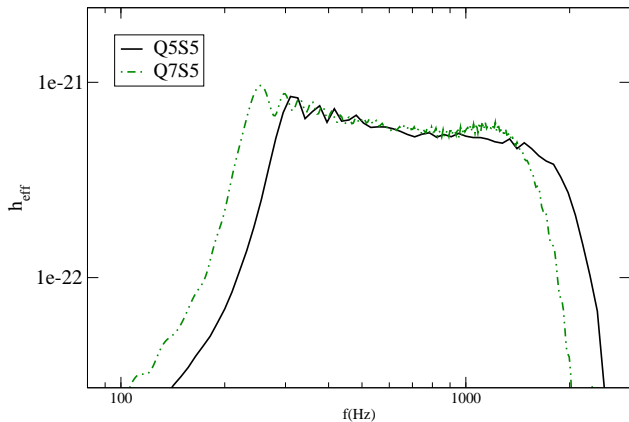

FIG. 10: Power spectrum of the gravitational wave signal for the low spin simulations ($a_{BH}/M_{BH} = 0.5$) for mass ratios $q = (5, 7)$.

ratio has a behavior similar to the $q = 7$, $a_{BH}/M_{BH} = 0.7$ case: both configurations have similar tidal disruption history, with a few percent of the mass being ejected in a tidal tail and the rest of the neutron star merging quickly with the black hole. The signal in the lower mass case ($q = 5$) is simply at a slightly higher frequency.

It is worth noting that similar differences can also be due to changes in the radius of the neutron star [7–10]. In order to extract information from that high-frequency signal, it is thus important to already have good estimates of the parameters of the binary to break that degeneracy. Given accurate gravitational wave templates, this can be obtained from the signal at lower frequency, during the orbital evolution.

V. LIMITS ON DISK FORMATION AND GAMMA-RAY BURSTS

All the simulations presented in this paper use fairly large stars, with $R_{NS} = 14.4\,\mathrm{km}$ for $M_{NS} = 1.4\,M_\odot$. They corre-

spond to particularly favorable cases for disk formation. They thus allow us to deduce limits on the minimum spin required to form significant accretion disks, at least if we assume that real neutron stars have radii $R_{NS} < 14.4\,\mathrm{km}$ (as predicted by Hebeler et al. [45]). Numerical simulations of BHNS using nearly the same nuclear equation of state have already been carried at lower mass ratios by Etienne et al. [5], as well as in our previous paper [6]. From these results, we notice that the behavior observed here in the cases $q = 5$, $a_{BH}/M_{BH} = 0.5$ and $q = 7$, $a_{BH}/M_{BH} = 0.7$ is very similar to the results obtained for $q = 3$, $a_{BH}/M_{BH} = 0.0$ [5, 6]: the amount of matter remaining outside the black hole at late times is $M_{out}/M_{NS} \sim 0.05 - 0.06$. However, these three cases are not exactly equivalent, of course. The higher mass ratio corresponds to a larger, lower density disk, which generally appears less favorable to the generation of SGRBs. Nonetheless, all the cases lead to a stable accretion disk of relatively low mass. Similarly, we have three cases for which nearly the entire star is quickly accreted onto the black hole, with a small but measurable amount of material ejected in a tidal tail $M_{out}/M_{NS} \sim 0.005 - 0.008$: the $q = 7$, $a_{BH}/M_{BH} = 0.5$ case presented here, as well as the $q = 5$, $a_{BH}/M_{BH} = 0.0$ and $q = 3$, $a_{BH}/M_{BH} = -0.5$ cases of Etienne et al. [5]. We thus have two curves in the space of black hole masses and spins giving us cases where the amount of matter available at late time for a $R_{NS} = 14.4\,\mathrm{km}$, $M_{NS} = 1.4 M_\odot$ star is $\sim 0.01 M_\odot$ and $\sim 0.08 M_\odot$ respectively (see Fig. 11). Below the lowest curve of Fig. 11, no significant disruption of the neutron star occurs before merger. Tidal effects are likely to affect the gravitational wave signal slightly, but the formation of an accretion disk is not possible. Above the highest curve, massive disks are formed for this particular stellar radius. However, all that can be said is that massive disks are possible: the more compact the neutron star, the more these curves would be displaced toward higher black hole spins. Finally, in between the two curves, we form a low mass disk of fairly low density or just a tidal tail containing a few percent of the initial neutron star mass and slowly falling back onto the central black hole.

In order for a BHNS binary to generate a short gamma-ray burst, a necessary condition would thus be to lie in the upper region of Fig. 11. This is not, however, sufficient. More compact stars make it more difficult to form accretion disks(see e.g. [48] for a model based on earlier, lower mass ratio simulations), and the same is true if the spin of the black hole and the orbital angular momentum are not aligned, as shown in Foucart et al. [6] for $q = 3$ mass ratios. In [6], the effect of spin misalignment was fairly limited, but we were considering configurations for which even a nonspinning black hole led to the formation of a significant accretion disk. Nevertheless, the final disk mass appeared to depend on the aligned component of the black hole spin. There is no guarantee that this will still be true for higher mass ratio, or for nearly extremal spins; further numerical studies in a general relativistic framework will be necessary to determine the effect of spin misalignment in BHNS binaries for $q \sim 7 - 10$. But if the same pattern holds for $q = 7$ and $q = 3$, misalignment angles $\sim 40°$ would be enough to have a BHNS with spin $a_{BH}/M_{BH} = 0.9$ behave

FIG. 11: Simulations with similar mass remaining outside the black hole for various BH masses and spins. All simulations correspond to $M_{NS} = 1.4M_\odot$, $R_{NS} = 14.4$ km (although a rescaling of M_{NS}, R_{NS} and M_{BH} would lead to the same fraction of the stellar mass remaining at late time). They thus correspond to optimistic predictions for the formation of accretion disks.
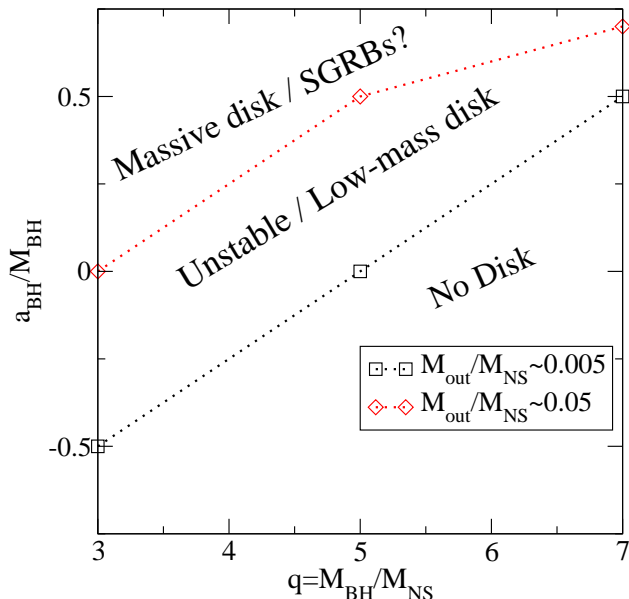
as an aligned configuration with $a_{BH}/M_{BH} = 0.7$. As misalignment angles of $\sim 40°$ could be fairly common [14], this would affect the probability that BHNS mergers form massive accretion disks.

We should also note that BHNS binaries which do not form an accretion disk could still emit a detectable electromagnetic signal before the disruption of the neutron star, for example in the form of resonant shattering precursor flares [49].

VI. CONCLUSION

Population synthesis models indicate that existing simulations of BHNS mergers in general relativity have probably studied black holes with masses below the most common astrophysical values. Binaries with lower mass black holes could occur, and their study has already offered valuable insights into the influence of various binary parameters such as BH spin, NS equation of state and mass ratio on the emitted gravitational wave signal and the disk formation process. However, studies of the behavior of BHNS binaries for more massive black holes are necessary if we want to obtain more accurate predictions for what is likely to be a significant portion of the available BHNS parameter space.

In this paper, we present the first simulations of BHNS binaries with $M_{BH} = 10M_\odot$. We show that, as opposed to what was found for lower mass black holes, the tidal disruption of the neutron star and the formation of an accretion disk are no longer the norm. We only observe significant accretion disks for high black hole spins, $a_{BH}/M_{BH} \geq 0.7$, and this result is

obtained using a fairly large neutron star ($R_{NS} \sim 14.4$ km), thus providing a likely lower bound on the spin required to form accretion disks in such systems.

As spin-orbit misalignment also inhibits disk formation [6], it appears that the formation of massive accretion disks will be a common result of BHNS mergers only if large black hole spins aligned with the orbital angular momentum are frequent, or if black holes in BHNS binaries are less massive than expected. This is of course of particular importance when determining whether BHNS mergers can be the progenitors of short gamma-ray bursts. BHNS systems with $M_{BH} \sim 10M_\odot$ and $a_{BH}/M_{BH} \leq 0.7$ appear to be unlikely candidates to power SGRBs. In Sec. V, we used existing simulations of BHNS binaries for mass ratios $q = 3 - 7$ to obtain approximate lower bounds for the magnitude of the black hole spin required to obtain massive disks.

BHNS systems with $M_{BH} \geq 7M_{NS}$ show another difference with respect to previously studied binaries: for high black hole spins $a_{BH}/M_{BH} \sim 0.9$, a few percent of the NS is either unbound or weakly bound. This could lead to the ejection of neutron-rich material in the neighborhood of the binary. However, study of this effect will require the use of numerical methods that resolve the evolution of the tidal tail better than our current code.

We showed that we can extract gravitational waves with a cumulative phase error $\Delta\phi < 0.2$ rad over about five orbits, without applying any time or phase shift to the signal. When matching the time and phase of the signal at its peak, our accuracy is similar to that reported by Kyutoku et al. [7] for lower mass black holes. The gravitational wave signal shows that as the spin of the black hole decreases, the spectrum goes through three regimes. At high spins, the spectrum is cut off at low frequency as the star is disrupted and the remaining material forms a nearly axisymmetric accretion disk. For intermediate spins, the spectrum is mostly flat, extending to frequencies ~ 2 kHz at which disruption leads to the formation of a thin tidal tail. At low spins, the spectrum is very similar to the signal from BH-BH binaries, where tidal disruption does not occur.

The behavior of BHNS binaries for higher mass ratios ($q > 7$) or smaller stellar radii should be even more similar to BH-BH binaries, with small corrections for the tidal distortion of the star. Whether any such binary can form an accretion disk will depend on how mergers occur for quasi-extremal spins, and how frequent high-spin black holes are in BHNS binaries. For high-spin systems, the relative alignment of the black hole spin and the orbital angular momentum is also likely to play an important role. In an earlier study of BHNS binaries with misaligned spins [6], we found that the qualitative effect of misalignment was relatively modest, but so were the effects of the spin itself, as even a nonspinning BH led to the formation of an accretion disk. At high mass ratios, it is likely that tidal tail and disk formation will only be possible for small spin-orbit misalignments, as is also predicted by Newtonian simulations [19]. Additional simulations will, however, be necessary to obtain more accurate predictions for such systems.

[1] LIGO Scientific Collaboration, http://www.ligo.caltech.edu.
[2] EGO-VIRGO Scientific Collaboration, http://www.ego-gw.it.
[3] W. H. Lee and E. Ramirez-Ruiz, New Journal of Physics **9**, 17 (2007), arXiv:astro-ph/0701874.
[4] M. Shibata and K. Uryu, Phys. Rev. **D74**, 121503 (2006), gr-qc/0612142.
[5] Z. B. Etienne, Y. T. Liu, S. L. Shapiro, and T. W. Baumgarte, Phys. Rev. **D79**, 044024 (2009).
[6] F. Foucart, M. D. Duez, L. E. Kidder, and S. A. Teukolsky, Phys.Rev.D **83**, 024005 (2011), 1007.4203.
[7] K. Kyutoku, H. Okawa, M. Shibata, and K. Taniguchi, Phys. Rev. D **84**, 064018 (2011).
[8] M. Shibata, K. Kyutoku, T. Yamamoto, and K. Taniguchi, Phys. Rev. **D79**, 044030 (2009), 0902.0416.
[9] M. D. Duez, F. Foucart, L. E. Kidder, C. D. Ott, and S. A. Teukolsky, Classical and Quantum Gravity **27**, 114106 (2010), 0912.3528.
[10] K. Kyutoku, M. Shibata, and K. Taniguchi, Phys.Rev.D **82**, 044049 (2010), 1008.1460.
[11] B. C. Stephens, W. E. East, and F. Pretorius, Astroph. J. Letters **737**, L5+ (2011), 1105.3175.
[12] S. Chawla, M. Anderson, M. Besselman, L. Lehner, S. L. Liebling, P. M. Motl, and D. Neilsen, Physical Review Letters **105**, 111101 (2010), 1006.2839.
[13] M. D. Duez, Classical and Quantum Gravity **27**, 114002 (2010), 0912.3529.
[14] K. Belczynski, R. E. Taam, E. Rantsiou, and M. van der Sluys, Astrophys. J. **682**, 474 (2008), arXiv:astro-ph/0703131.
[15] K. Belczynski, M. Dominik, T. Bulik, R. O'Shaughnessy, C. Fryer, and D. E. Holz, Astroph.J.Letters **715**, L138 (2010), 1004.0386.
[16] W. H. Lee and W. Kluzniak, Astrophys. J. **526**, 178 (1999), astro-ph/9808185.
[17] H. Janka, T. Eberl, M. Ruffert, and C. L. Fryer, Astrophys. J. Lett. **527**, L39 (1999), arXiv:astro-ph/9908290.
[18] S. Rosswog, Astrophys. J. **634**, 1202 (2005), arXiv:astro-ph/0508138.
[19] E. Rantsiou, S. Kobayashi, P. Laguna, and F. A. Rasio, Astrophys. J. **680**, 1326 (2008), arXiv:astro-ph/0703599.
[20] SpEC Collaboration, http://www.black-holes.org/SpEC.html.
[21] M. D. Duez, F. Foucart, L. E. Kidder, H. P. Pfeiffer, M. A. Scheel, and S. A. Teukolsky, Phys. Rev. D **78**, 104015 (2008), 0809.0002.
[22] L. Lindblom, M. A. Scheel, L. E. Kidder, R. Owen, and O. Rinne, Class. Quant. Grav. **23**, S447 (2006).
[23] X.-D. Liu, S. Osher, and T. Chan, Journal of Computational Physics **115**, 200 (1994), ISSN 0021-9991.
[24] G.-S. Jiang and C.-W. Shu, Journal of Computational Physics **126**, 202 (1996), ISSN 0021-9991.
[25] R. Borges, M. Carmona, B. Costa, and W. S. Don, Journal of Computational Physics **227**, 3191 (2008), ISSN 0021-9991.
[26] B. v. L. A. Harten, P. D. Lax, SIAM Rev. **25**, 35 (1983).
[27] W. H. Press, S. A. Teukolsky, W. T. Vetterling, and B. P. Flannery, *Numerical Recipes: The Art of Scientific Computing* (Cambridge University Press, 2007), 3rd ed.
[28] K. Gustaffson, ACM Transactions on Mathematical Software **17**, 533 (1991).
[29] E. Hairer, S. Norsett, and G. Wanner, *Solving Ordinary Differential Equations II. Stiff and Differential-Algebraic Problems* (New York:Springer, 1996), 2nd ed.
[30] G. Soderlind, ACM Transactions on Mathematical Software **29**, 1 (2003).
[31] M. Boyle, Phys. Rev. D **84**, 064013 (2011).
[32] I. MacDonald, S. Nissanke, and H. P. Pfeiffer, Classical and Quantum Gravity **28**, 134002 (2011), 1102.5128.
[33] J. S. Read, C. Markakis, M. Shibata, K. Uryū, J. D. E. Creighton, and J. L. Friedman, Phys. Rev. D **79**, 124033 (2009), 0901.3258.
[34] T. Regge and J. A. Wheeler, Physical Review **108**, 1063 (1957).
[35] F. J. Zerilli, Physical Review Letters **24**, 737 (1970).
[36] O. Sarbach and M. Tiglio, Phys. Rev. D **64**, 084016 (2001), arXiv:gr-qc/0104061.
[37] O. Rinne, L. T. Buchman, M. A. Scheel, and H. P. Pfeiffer, Classical and Quantum Gravity **26**, 075009 (2009), 0811.3593.
[38] B. Szilágyi, L. Lindblom, and M. A. Scheel, Phys. Rev. D **80**, 124010 (2009), 0909.3557.
[39] H. P. Pfeiffer, L. E. Kidder, M. A. Scheel, and S. A. Teukolsky, Comput. Phys. Commun. **152**, 253 (2003).
[40] F. Foucart, L. E. Kidder, H. P. Pfeiffer, and S. A. Teukolsky, Phys. Rev. **D77**, 124051 (2008).
[41] J. W. York, Phys. Rev. Lett. **82**, 1350 (1999).
[42] H. P. Pfeiffer, Ph.D. thesis, Cornell University (2003), arXiv:gr-qc/0510016v1.
[43] G. Lovelace, R. Owen, H. P. Pfeiffer, and T. Chu, Phys. Rev. **D78**, 084017 (2008).
[44] H. P. Pfeiffer, D. A. Brown, L. E. Kidder, L. Lindblom, G. Lovelace, and M. A. Scheel, Classical and Quantum Gravity **24**, S59 (2007), arXiv:gr-qc/0702106.
[45] K. Hebeler, J. M. Lattimer, C. J. Pethick, and A. Schwenk, Physical Review Letters **105**, 161102 (2010), 1007.1746.
[46] L. Rezzolla, Classical and Quantum Gravity **26**, 094023 (2009), 0812.2325.
[47] Y. Zlochower, M. Campanelli, and C. O. Lousto, Classical and Quantum Gravity **28**, 114015 (2011), 1011.2210.

[48] F. Pannarale, A. Tonita, and L. Rezzolla, Astrophys. J. **727**, 95 (2011), 1007.4160.

[49] D. Tsang, J. S. Read, T. Hinderer, A. L. Piro, and R. Bondarescu, Physical Review Letters **108**, 011102 (2012), 1110.0467.

[50] C. Catlett et al., in *Advances in Parallel Computing*, edited by L. Grandinetti (IOS press, Amsterdam, 2007).